Edinburgh Research Explorer

Tri-mode optical biopsy probe with fluorescence endomicroscopy, Raman spectroscopy, and time-resolved fluorescence spectroscopy

Tri-mode optical biopsy probe with fluorescence endomicroscopy, Raman spectroscopy, and time-resolved fluorescence spectroscopy

Harry Alexander Charles Wood *, 1, 2 | Katjana Ehrlich 2, 3 | Stephanos Yerolatsitis 1, 2, 4 | András Kufcsák 2 | Tom Michael Quinn 2 | Susan Fernandes 2 | Dominic Norberg 2 | Nia Caitlin Jenkins 2 | Vikki Young 2 | Irene Young 2 | Katie Hamilton 2 | Sohan Seth 2 | Ahsan Akram 2 | Robert Rodrick Thomson 2, 3 | Keith Finlayson 2 | Kevin Dhaliwal 2 | James Morgan Stone 1, 2

1 Centre for Photonics and Photonic Materials, University of Bath, Bath, BA27AY, UK

2 Translational Healthcare Technologies Group, Centre for Inflammation Research, Queen's Medical Research Institute, University of Edinburgh, 47 Little France Crescent, Edinburgh, EH164TJ, UK

3 Scottish Universities Physics Alliance (SUPA), Institute of Photonics and Quantum Science, Heriot-Watt University, Edinburgh, EH144AS, UK

4 The College of Optics and Photonics (CREOL), University of Central Florida, Orlando, Florida 32816, USA

* Correspondence

Dr. Harry Alexander Charles Wood, Department of Physics, University of Bath, Claverton Down, Bath, BA27AY, UK

Email: h.wood@bath.ac.uk

We present an endoscopic probe that combines three distinct optical fibre technologies including: A high-resolution imaging fibre for optical endomicroscopy, a multimode fibre for time-resolved fluorescence spectroscopy, and a hollow-core fibre with multimode signal collection cores for Raman spectroscopy. The three fibres are all enclosed within a 1.2 mm diameter clinical grade catheter with a 1.4 mm end cap.

To demonstrate the probe's flexibility we provide data acquired with it in loops of radii down to 2 cm. We then use the probe in an anatomically accurate model of adult human airways, showing that it can be navigated to any part of the distal lung using a commercial bronchoscope. Finally, we present data acquired from fresh *ex vivo* human lung tissue.

Our experiments show that this minimally invasive probe can deliver real-time optical biopsies from within the distal lung - simultaneously acquiring co-located high resolution endomicroscopy and biochemical spectra.

KEYWORDS

Micro endoscopy, Raman endoscopy, fluorescence endomicroscopy, time-resolved fluorescence spectroscopy
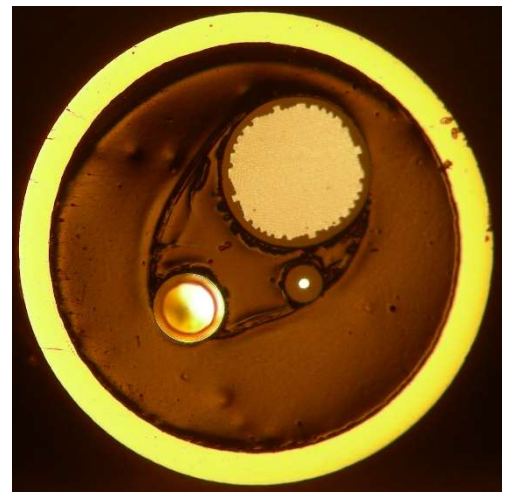
1 | INTRODUCTION

Endoscopy has been a key method of non-invasive disease diagnosis since its conception in the 19th century [1], and even more so after the invention of the flexible optical fibre bundle [2]. Since then, the probes have drastically decreased in size [3, 4], increased in resolution [5-7], and techniques such as optical coherence tomography [8] and scanning 2-photon fluorescence [9] have enabled 3-dimensional image acquisition. Optical endomicroscopy (OEM) technologies now provide cellular-resolution imaging in real-time, empowering clinicians to carry out preliminary diagnoses *in vivo* [10]. Ultimately it is hoped that such minimally invasive optical biopsy techniques will augment traditional biopsy and histopathology pathways and expedite clinical workflows.

Optical biopsy research has recently broadened to include spectroscopic methods of tissue characterisation [11-15], with one of the most prevalent being Raman spectroscopy. Raman scattering is the process by which light scatters inelastically and transfers energy to or from the acoustic modes of bonds. In any instance, the amount of energy exchanged is specific to the bond resonance, and so produces a unique shift in the

wavelength of the scattered light [16]. The depth and specificity of this information allows even subtle variations in protein structure to be distinguished [17-20], enabling clinically significant achievements such as discrimination between cancerous and healthy tissues [20-22]. Fluorescence spectroscopy is another key optical biopsy technique as it allows the energy states of fluorophores to be studied. This technique is often expanded upon by using time-resolved detectors to investigate the excited state lifetimes. Such Time-Resolved Fluorescence Spectroscopy (TRFS) techniques have also been used to differentiate between healthy and cancerous tissue [23, 24].

It is highly unlikely that any single optical biopsy method will achieve 100% sensitivity and specificity in clinical practice. This necessitates combined solutions of complementary technologies, such that any limitations inherent in one are overcome by the others. Recently several such devices capable of multiple optical tissue characterisation methods have been reported [25-27].

Here we report the production and application-oriented testing of a 1.4 mm diameter optical biopsy probe that features three distinct optical fibres for optical endomicroscopy (OEM), Raman spectroscopy, and TRFS. These three modalities were chosen for their complimentary nature: OEM for examining tissue architecture, cellular infiltration, and molecular imaging; TRFS for investigating the autofluorescence of molecules such as NADH and FAD, and aspects of their tissue's microenvironment such as temperature and pH; and Raman spectroscopy to probe the vibrational fingerprints of biomolecules.

We begin with a description of the probe's structure, then the structure and function of each optical fibre component, and their corresponding analysis setups. Following this, we demonstrate the probe's performance in extreme bending situations, then in an endoscopy simulation, and finally on healthy *ex vivo* human lung tissue. Because these datasets all originate from the same tissue with millimetre precision, collecting and analysing them in conjunction during interventional procedures will allow a critical level of redundancy, certainty, and specificity to be achieved.

2 | PROBE DESCRIPTION

2.1 | Probe structure

The central diagram in Figure 1 shows the overall structure of the 3-in-1 multifunctional optical fibre probe. Starting from the proximal end, the three optical fibres are individually FC/PC terminated and the end faces polished for easy connection to their respective optical setups. Clear, biocompatible Pebax® tubing protects the first 0.9 m length of each fibre, at which point they meet within a PVC 3-to-1 splitter. The three fibres emerge from the single distal port of the splitter into a 1.4 m long, 1.2 mm diameter biocompatible multilayer polyimide and Pebax® tube with a stainless-steel

braid for structural strength. The distal tip of the probe is reinforced with an epoxy-filled, 4 mm long, 1.4 mm outer diameter stainless-steel tube. The slight separation of the fibres means they sample from different regions within a 1.2 mm boundary. If one fibre detects a tissue abnormality the device can be repositioned. Figure 1e shows the probe's distal end face, polished flat, and steel edge chamfered. A maximum diameter of 1.4 mm allows us to guide the probe using the working channels of commercial bronchoscopes and enables access to the tiny bronchioles of the distal human lung.

2.2 | Optical fibres

We fabricated all the probe's optical fibre components using the drawing towers at the University of Bath's Centre for Photonics and Photonic Materials. Two kinds of stock glass were used; the undoped silica tubes and rods were Superasil F300 (Heraeus), and the germanium doped silica was from OM1 preforms with a core to cladding ratio of 0.75, parabolic index profile, and 0.3 peak numerical aperture (Draka, Prysmian). Both materials are mass produced for the telecoms industry, supporting cost-effective probe production, potentially as a single-use medical product. This would subvert the need to clean the probes between clinical procedures, reducing workload, cross infection, and probe degradation.

Figures 1a-d are optical micrographs of the polished or cleaved end faces of each fibre. Figure 1a shows the imaging fibre for OEM, the design of which is a development of our previously published square array fibre [28], redesigned here for more efficient use of the cross-section area. This new version provides 9425 cores and a 35% larger field-of-view within a 450 μm diameter fibre that is 17% thinner than the previous version. We arrange the cores such that no nearest neighbours have the same diameter, minimising core crosstalk to maximise image quality [29]. Figure 1b shows the end face of the 35 μm core diameter multimode fibre we use for TRFS. The multimode endcap and the cleaved cross section of the fibre used for Raman spectroscopy are shown in Figures 1c and d, respectively. The Raman fibre is more fully described and evaluated in [30, 31]. A central ring of air-filled capillaries forms an open-boundary single-mode negative-curvature hollow-core to deliver 785 nm excitation light to the distal end. This reduces the Raman background signal from the glass by a factor of 10^4. The surrounding ring of 8 large multimode cores collect and return the sample's Raman signal. By introducing the multimode cores, we tripled the collection efficiency of the system (without a significant increase to the silica Raman background) compared to using a standard negative-curvature fibre [31]. To prevent ingress of fluids into the hollow structure, we splice a short piece of multimode fibre onto the distal end and polish it back to a window that is less than 0.3 mm thick, minimising the background signal it generates [30].
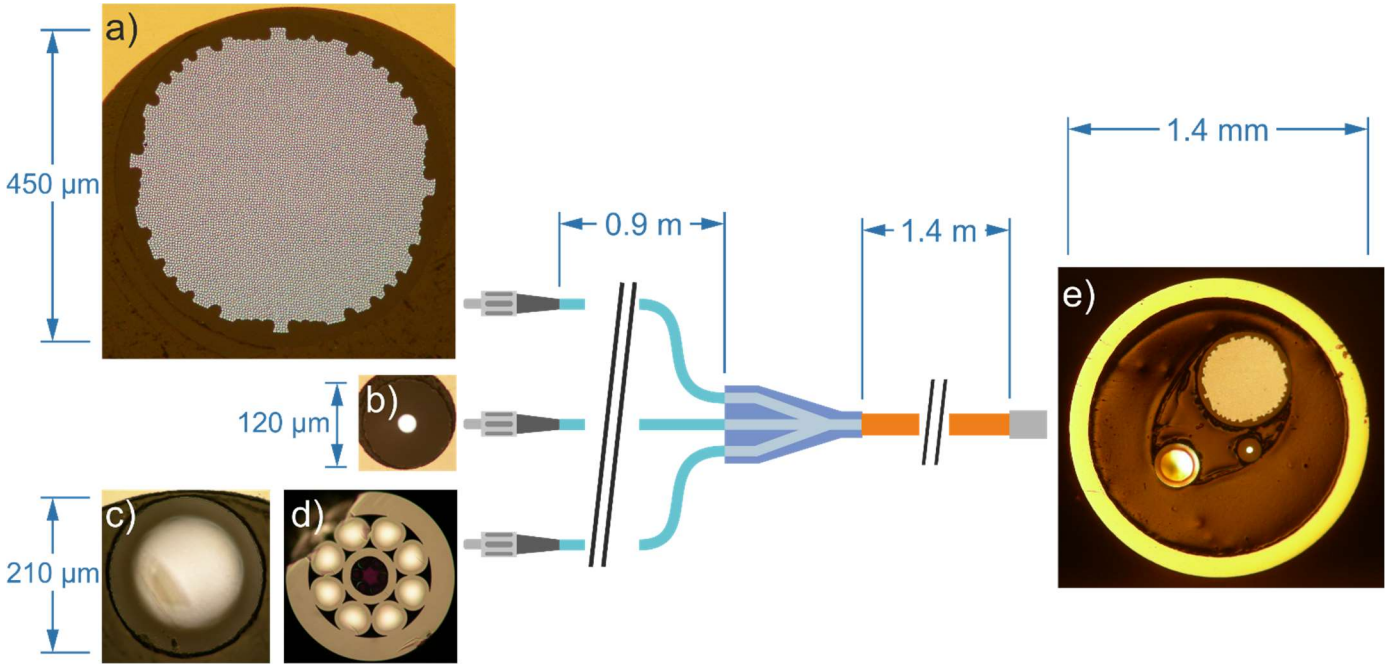
FIGURE 1 A structural diagram of the probe, including cross section images of each of the component optical fibres. The proximal end (left) of each fibre is terminated in an FC connector and protected along its length by a 0.9 m long clear Pebax tube to where they meet within the plastic 3-to-1 splitter (centre). From here to the distal tip (right) the three-fibre bundle is protected within a 1.4 m long multi-layer braided tube of 1.2 mm outer diameter, shown in orange. At the distal tip the fibres are glued within a thin 1.4 mm diameter stainless-steel ferule to allow the end face to be finely polished. a) Imaging fibre. b) Multimode fibre for time-resolved fluorescence spectroscopy. c) The end cap used to seal the Raman fibre. d) Fibre for Raman spectroscopy, including a central hollow core surrounded by solid multimode signal collection cores. e) The distal end face of the probe.

2.3 | Optical systems

By terminating the proximal fibre ends with FC/PC connectors we can easily and robustly couple them to their respective benchtop optical systems, and quickly swap to a new probe if the need arises. In this section we provide an outline of these optical systems, which are described in greater detail in their respective references.

We used a widefield fluorescence imaging system based on a 470 nm LED excitation source and a CMOS camera (GS3-U3-41C6NIR-C, FLIR, Point Grey) to produce high-resolution fluorescence endomicroscopy videos [32]. We packaged an equivalent system into an aluminium casing that is mounted on one level of a medical cart (Parity Medical's MedStore Plus Cart) for clinical use [32].

For time-resolved fluorescence sensing we coupled the multimode fibre to a system similar to that published in [33]. This consisted of three parts: (i) a 485 nm pulsed laser with a 20 MHz repetition rate and 200 µW average power, (ii) an optical coupling and collection system based on an epi-fluorescence microscope, (iii) a time-resolved spectrometer based on an array of CMOS single photon avalanche diodes (SPADs). All 512 pixels of the array record histograms of photon arrival times via the on-chip system [34]. For the data presented in this paper we used a time bin width (resolution) of 800 ps, which allows a 25.6 ns wide window to be recorded. We use a grating to obtain spectral information by dispersing the light across the detector.

We coupled the Raman fibre to a spectroscopy setup based on the one described by Yerolatsitis *et. al.* [30]. For excitation we used a continuous wave 785 nm 20 mW diode laser source, filtered to 1 nm bandwidth. We filtered the returning light to the Stokes scattered wavelengths using 785 nm long-pass and dichroic filters before analysing it with a commercial Raman spectrometer (QEPro Raman, Ocean Insight).

3 | EXPERIMENTAL DEMONSTRATION

3.1 | Minimum bend radius

Anatomical constraints impose a critical limit on the probe's minimum functional bend radius. This performance criterion is determined not only by mechanical characteristics, but also by optical effects such as bend loss. Therefore, each fibre's optical characteristics were investigated with incrementally tighter loops in the middle of the probe's distal length (containing all three fibres), down to its structural limit of 10 mm radius, as shown in Figure 2a.

To evaluate the imaging fibre, we first used a photodiode to monitor the intensity of the blue light emitted from the distal end during bending. No intensity change was measured, so we moved on to checking for image degradation. For this purpose, we chose a 1951 USAF test target backed by a green fluorescent slide as the imaging standard. Element 3 of group 7 (3.1 µm spacing) was equally visible at all tested bend radii (see Figure 2c), and no reduction in contrast was observed.
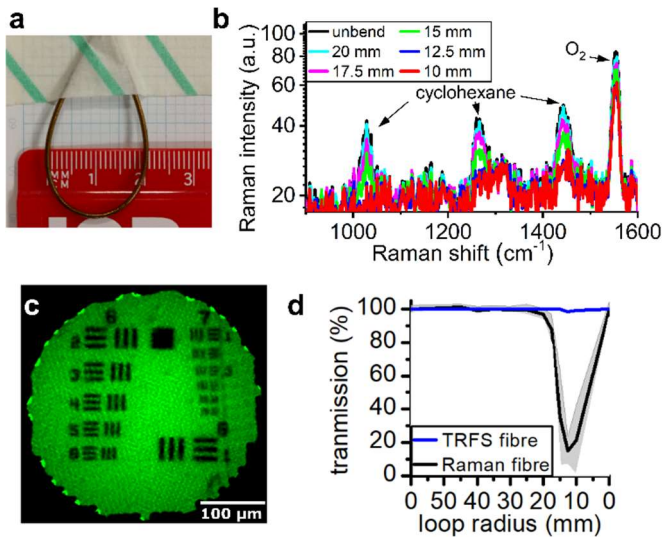
FIGURE 2 Data showing the performance of the probe at small bends. a) A photo of the probe bent into a loop of 10 mm minimum radius. The loop was started at 50 mm radius and made incrementally smaller while recording data using each of the three fibres. b) Raman spectra of cyclohexane using the Raman fibre and a 1 s acquisition with the probe loop radii listed in the inset. The additional peak at 1557 cm^{-1} is due to the molecular oxygen within the hollow-core fibre. c) A 1951 USAF resolution test target backed onto a fluorescent slide, imaged using the OEM fibre while the probe was in 10 mm radius loop. d) Plots of the TRFS and Raman fibre transmissions with the probe in loops of radii indicated on the bottom axis. The grey area around the curve indicates the standard deviation of 3 sets of results.

We immersed the distal tip of the probe in a 1 μM aqueous solution of fluorescein sodium to test the performance of the TRFS system during bending. As Figure 2d shows, we recorded no loss of returning fluorescent light.

Because hollow-core fibres typically have higher bend loss than solid core fibres [35, 36] we anticipated that the Raman fibre would be the first to fail optically under extreme bending. We began investigating its performance using a photodiode at the distal end to measure the bend loss of transmitted excitation light. We observed a sharp drop in transmission with bends smaller than 17.5 mm in diameter, but no long-term loss once the probe was unbent, as shown in Figure 2d. The slight rise in transmitted power at the 10 mm structural bend limit is likely due to resonant bend loss as bends perturb the propagation constants of modes in the hollow core fibre's capillary cladding [35, 36].

To investigate the effects of bending on the returning Raman signal, we immersed the probe's distal end in cyclohexane and took 10 s spectral acquisitions under the same range of bending conditions as before. The raw spectra produced are shown in Figure 2b, with the inset indicating the corresponding probe bend radius. Three of cyclohexane's characteristic Raman peaks at roughly 1030, 1260 and 1450 cm^{-1}, and one attributed to the molecular oxygen in the hollow core at 1557 cm^{-1}, are clear down to bend radii of 17.5 mm. As a functional bend limit, this does not preclude access to any branch of the adult human respiratory airway tree.

3.2 | Bronchoscopy simulation

Progressing towards the intended application in interventional pulmonology, we performed a bronchoscopy procedure using the working channel of a commercial bronchoscope (BF-H109, Olympus) to navigate our probe through a bronchoscopy training model that accurately represents human lung architecture (LM-092, Koken CO, Japan). This presented our probe with the same compound bends it would face in a clinical bronchoscopy procedure, passing into the oral cavity, intubating the trachea, and through the progressively narrower branching airways.

We began by navigating the more straightforward paths to the lower lung lobes, evaluating the probe's performance, then moving on to the more challenging upper lobes. In each instance we pushed the 5.4 mm diameter bronchoscope until it wedged, then slid our probe out of the 2.2 mm diameter working channel to progress, unguided, further into the distal bronchioles. Our probe easily passed through even the smallest lumen tested. Once it emerged from the open-ended rubber bronchioles, we presented it with the same test samples as in the minimum bend radius experiments.

The most tortuous path was to the apical segment of the right upper lobe [37], the results from which we present in Figure 3. With our probe positioned as in Figure 3a, we sequentially obtained the test target OEM image in Figure 3b from a live video feed, the TRFS data in Figures 3c and d from 6 s and 6 ms acquisitions, respectively, and the Raman spectra in Figure 3e from 10 s acquisitions. Element 1 of group 7 of the USAF test target is still visible (3.91 μm line width), indicating consistent imaging performance throughout the experiment. The fluorescence spectra and lifetime plots of the fluorescein solution show small changes compared to previous results, likely due to the inconsistency in placing the fluorescein sodium solution on the end of the probe while it was inside the lung model. The Raman spectra retain cyclohexane's three characteristic peaks and the molecular oxygen peak, demonstrating its ability to collect data from any lung lobe.

Critically, we observed no significant reduction in signal from any fibre in any of the paths, even in the apical segment of the right upper lobe.
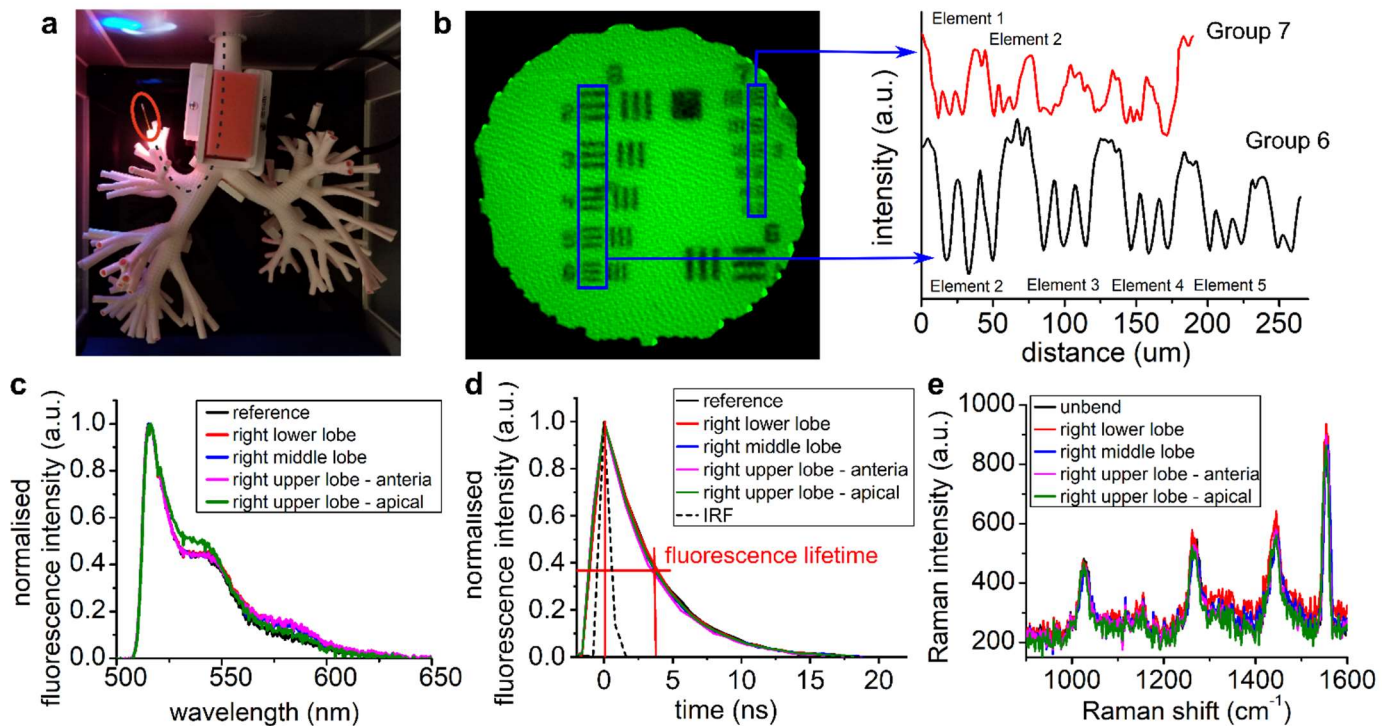
FIGURE 3 The probe's performance in a simulated bronchoscopy. a) Picture of the Koken rubber lung model with the tip of the probe (circled in red) emerging from the apical segment of the right upper lobe. The probe's path within the model and bronchoscope is traced by the dashed black line. b) An OEM image of a 1951 USAF resolution test target on fluorescent backing, placed at the probe's tip while in the position shown in a) and accompanying intensity profiles along groups 6 and 7. c) The fluorescence emission spectra of fluorescein sodium (1 μM concentration in PBS) placed at the probe's distal end. d) Plot of the fluorescein sodium solution's fluorescence decay. e) Raman spectra of cyclohexane and molecular oxygen using the probe.

3.3 | Human lung tissue optical biopsy

We used a whole *ex vivo* lobectomy specimen, as shown in Figure 4, to demonstrate the clinical compatibility and potential of our optical biopsy probe. The sample was obtained from a patient undergoing thoracic resection surgery for suspected lung cancer (NHS Lothian BioResource, Scotland Research Ethics Service, reference 15/ES/0094).

FIGURE 4 Image of an ex vivo human lung lobe being characterised by our probe by inserting it through a 20-gauge needle.

By inserting a 20-gauge spinal needle deep into the lung parenchyma, we were able to pass the probe down the needle bore until in direct contact with internal tissue. We then collected data with each of the optical fibre components sequentially at 5 different locations within the tissue per modality (15 total), the results of which are summarised in Figure 5. Figure 5a is a series of still images from the OEM videos, Figure 5b shows the Raman spectra, and Figure 5c is the time-resolved fluorescence intensity data and lifetimes. The full OEM videos and raw datasets are provided in the supplementary information and at [38].

No fluorescent markers were required for imaging as we used the lung tissue's endogenous fluorophores, such as elastin [39]. We processed this OEM data in real-time to remove background light and interpolate over the blank spaces between the cores [40]. This produced a live video feed of the sample's healthy lung tissue structure, shown in Figure 5a. Features of these images that indicate the sample's good health include the clear bright strands of elastin rich fibrous tissue, interspersed by gas filled alveolar pores and ducts that appear as dark spaces between the connecting tissue. Such techniques have previously been used to identify distal lung pathologies by the associated disruption to the alveolar network [41].
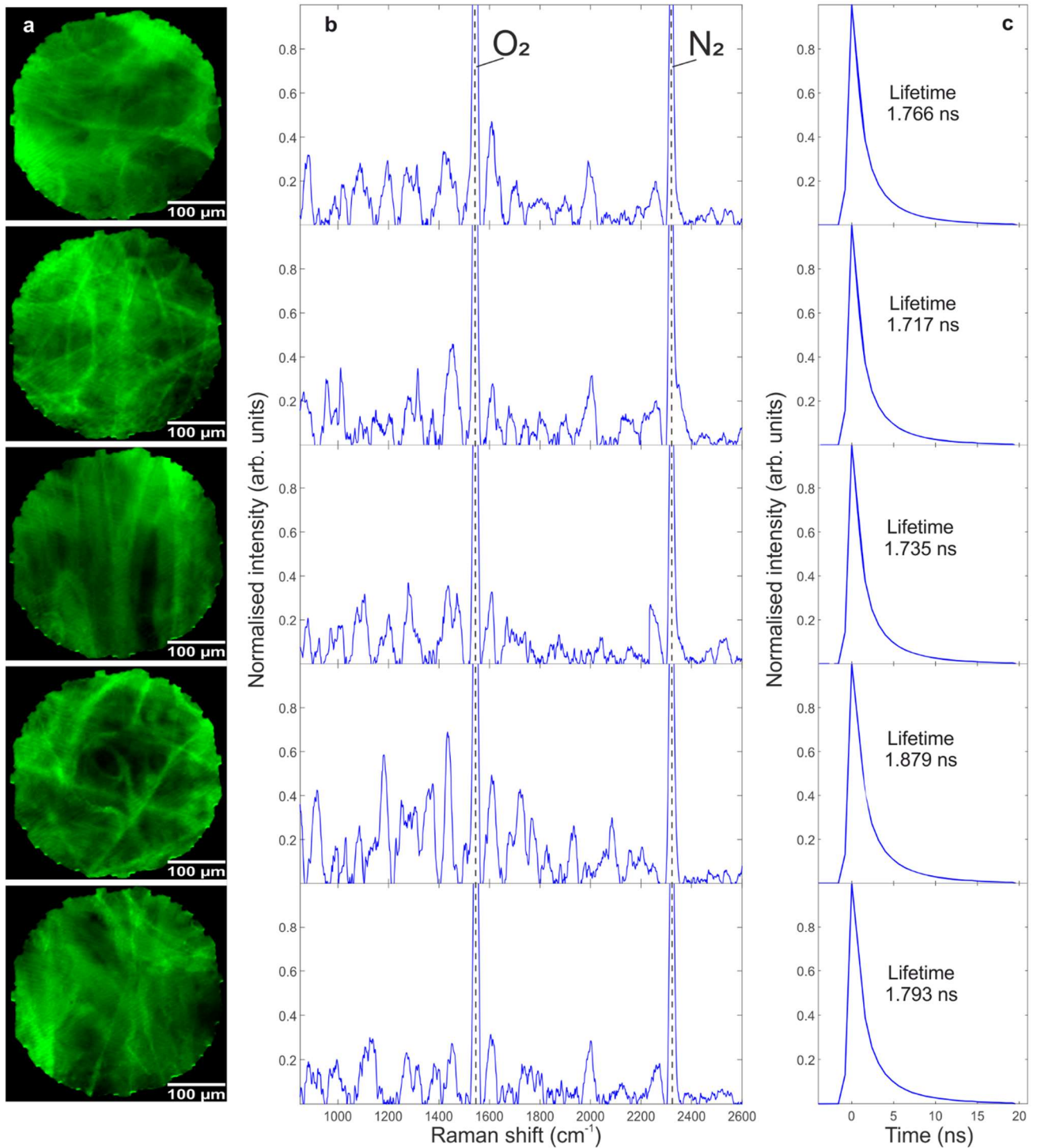
FIGURE 5 a) OEM images b) Raman spectra and c) TRFS spectra of an *Ex vivo* human lobectomy specimen characterised by our probe. We used a 20-gauge spinal needle to insert the probe into the lobe and characterise the internal tissue using each technique in sequence at different locations. The OEM data was processed in real-time to produce a live video of the tissue's structure, from which we extracted the example images a). The Raman spectra b) were each obtained using 2 sequential 5 s acquisitions and the SERDS [30] processing method to remove the fluorescent background. Using the TRFS system to extract the change in fluorescence intensity in time produces the traces shown in c), all indicating a fluorescent lifetime between 1.7 and 1.9 ns.

Strongly fluorescent tissue is not without its challenges – it can easily overwhelm a weak signal such as Raman scattered light. For this reason, we employed a Shifted Excitation Raman Difference Spectroscopy (SERDS) method in conjunction with our probe's Raman system. In summary, by using two excitation sources with slightly different wavelengths, a pair of spectra are produced where the Raman signatures are shifted correspondingly, but the fluorescence background remains constant in both. By subtracting one from the other, the fluorescence signal is cancelled while the original Raman spectrum can be restored from the difference spectrum. However, as the fluorescence contribution often varies in the two raw spectra, additional processing steps are required to get clean Raman signatures, these are more fully described in [30, 42]. Here, we recorded spectra in 5 s long acquisitions, using two laser sources thermally tuned to 784 and 785 nm. We applied the same processing pipeline as described by Yerolatsitis *et. al.* [30], except for the step to reconstruct the Raman spectrum from the difference spectrum, where we instead applied boxcar integration by summing the difference spectrum at two neighbouring sampling points. This process resulted in Raman spectra as shown in Figure 5b. The sharp molecular oxygen and nitrogen peaks are present in each of the five spectra, as well as peaks at roughly 1005 cm^{-1} and 1300 cm^{-1} that are potentially attributed to elastin and collagen [17, 18]. Due to variations between samples, full characterisation of the Raman spectra will require extensive data sets from many different patients to accumulate a list of significant peaks and their associated biochemistry, supported by appropriate statistics.

We used the TRFS system to interrogate the spectral and temporal profiles of the tissue's autofluorescence. The intensity/time/wavelength data we obtained were summed across the wavelength range and fit with a single exponential curve using a least-square method, producing Figure 5c. This shows that the tissue at each location shares similar fluorescent decay profiles and lifetimes between 1.7 and 1.9 ns, consistent with previous reported values [43, 44].

4 | CONCLUSION

We have a built a 1.4 mm diameter endoscopic probe that provides three complementary optical datasets with sub-millimetre co-location. To show that the probe is clinically viable we have carried out extensive bend loss experiments, model bronchoscopy procedures, and characterised a fresh *ex vivo* human lung tissue sample. The probe operated to a minimum bend radius of 17.5 mm, was capable of the compound bends needed to navigate human airways, and was sufficiently sensitive to retrieve detailed imaging, fluorescence, and Raman data from human tissue.

This probe platform is ready to be evaluated in larger tissue banks including lung cancer samples and translated for clinical evaluation for safety and performance evaluation in interventional pulmonology procedures. The probe can also be adapted to suit other organs and tissues by including other sensing or imaging fibres and devices, capillaries for fluid delivery and extraction, or micromechanical tools. Other organs may have more strict outer diameter requirements, but

by omitting the imaging fibre the probe could be made thinner than one millimetre [30], while still providing a full suite of chemically specific spectra.

This minimally invasive optical biopsy probe provides rapid *in situ* structural and chemical information, potentially augmenting the diagnostic yield of existing endoscopic approaches by enabling real-time optical biopsies and highly targeted conventional biopsies.

DATA AVAILABILITY STATEMENT

The data that support the findings of this study are openly available in [38] at https://doi.org/10.15125/BATH-01174.

REFERENCES

[1] P. Bozzini, *Journal of Practical Medicine and Surgery*, **1806**, *24*, 107

[2] H. H. Hopkins, and N. S. Kapany, *Nature*, **1954**, *173*, 39.

[3] W. Burnett, *Gut*, **1962**, *3*, 361.

[4] A. F. Gmitro, and D. Aziz, *Optics Letters*, **1992**, *18*, 565.

[5] H. A. C. Wood, K. Harrington, T. A. Birks, J. C. Knight, and J. M. Stone, *Optics Letters*, **2018**, *43*, 5311.

[6] C. M. Lee, C. J. Engelbrecht, T. D. Soper, F. Helmchen, and E. J. Siebel, *Journal of Biophotonics*, **2010**, *3*, 385.

[7] M. A. Mooney, A. H. Zehri, J. F. Georges, and P. Nakaji, *Neurosurgical Focus*, **2014**, *36*, 1.

[8] J. G. Fujimoto, M. E. Brezinski, G. J. Tearney, S. A. Boppart, B. Bouma, M. R. Hee, J. F. Southern, and E. A. Swanson, *Nature Medicine*, **1995**, *1*, 970.

[9] B. N. Ozbay, G. L. Futia, M. Ma, V. M. Bright, J. T. Gopinath, E. G. Hughes, D. Restrepo, and E. A. Gibson, *Scientific Reports*, **2018**, *8*, 1.

[10] R. C. Newton, S. V. Kemp, P. L. Shah, D. Elson, A. Darzi, K. Shibuya, and S. Mulgrew, G-Z. Yang, *Lung*, **2011**, *189*, 111.

[11] U. Bindig, I. Gersonde, M. Meinke, Y. Becker, and G. Muller, *Spectroscopy*, **2003**, *17*, 323.

[12] S. Kino, S. Omori, T. Katagiri, and Y. Matsuura, *Biomedical Optics Express*, **2016**, *7*, 701.

[13] J. C. C. Day, R. Bennett, B. Smith, C. Kendall, J. Hutchings, G. M. Meaden, C. Born, S. Yu, and N. Stone, *Physics in Medicine and Biology*, **2009**, *54*, 7077.

[14] C. A. Ross, D. G. MacLachlan, B. J. E. Smith, R. J. Beck, J. D. Shephard, N. Weston, and R. R. Thomson, *Micromachines*, **2020**, *11*, 1.

[15] I. J. Bigio, and J. R. Mourant, *Physics in Medicine and Biology*, **1997**, *42*, 803.

[16] C. V. Raman, and K. S. Krishnan, *Nature*, **1928**, *122*, 12.

[17] I. Notingher, S. Verrier, H. Romanska, A. E. Bishop, J. M. Polak, and L. L. Hench, *Spectroscopy*, **2002**, *16*, 43.

[18] Z. Movasaghi, S. Rehman, and I. U. Rehman, *Applied Spectroscopy Reviews*, **2007**, *42*, 493.

[19] A. G. Berger, N. J. Crane, and E. A. Elster, *Proc. SPIE: Optical Diagnositcs and Sensing*, **2016**, *9715*.

[20] Z. Huang, S. K. Teh, W. Zheng, J. Mo, K. Lin, X. Shao, K. Y. Ho, M.Teh, and K. G. Yeoh, Optics Letters, **2009**, 34, 758.

[21] M. B. Fenn, P. Xanthopoulos, G. Pyrgiotakis, S. R. Grobmyer, P. M. Pardalos, and L. L. Hench, *Advances in Optical Technologies*, **2011**, *2011*, 1.

[22] Z. Huang, A. McWilliams, H. Lui, D. I. McLean, S. Lam, and H. Zeng, *International Journal of Cancer*, **2003**, *107*, 1047.

[23] D. Farwell, J. Meier, J. Park, Y. Sun, H. Coffman, B. Poirier, J. Phipps, S. Tinling, D. Enepekides, and L. Marcu, *Arch Otolaryngol Head Neck Surgery*, **2010**, *136*, 126.

[24] A. Cosci, M. S. Nogueira, S. Prataviera, A. Takahama Jr, R. S. Azevedo, and C. Kurachi, *Biomedical Optics Express*, **2018**, *9*, 648.

[25] J. L. Lagarto, V. Shcheslavskiy, F. S. Pavone, and R. Cicchi, *Optics Letters*, **2020**, *45*, 2247.

[26] B. E. Sherlock, J. E. Phipps, J. Bec, and L. Marcu, *Optics Letters*, **2017**, 42, 3753

[27] S. Dochow, D. Ma, I. Latka, T. Bocklitz, B. Hartl, J. Bec, H. Fatakdawala, E. Marple, K. Urmey, S. Wachsmann-Hogiu, M. Schmitt, L. Marcu, and J. Popp, *Analytical and Bioanalytical Chemistry*, **2015**, 407, 8291

[28] J. M. Stone, H. A. C. Wood, K. Harrington, and T. A. Birks, *Optics Lett*ers, **2017**, *42*, 1484

[29] X. Chen, K. L. Reichenbach, and C. Xu, *Optics Express*, **2008,** *16*, 21598.

[30] S. Yerolatsitis, A. Kufcsák, K. Ehrlich, H. Wood, S. Fernandes, T. Quinn, V. Young, I. Young, K. Hamilton, A. Akram, R. Thomson, K, Finlayson, K. Dhaliwal, and J. Stone, *Journal of Biophotonics*, **2021**, *14*, 10, e202000488.

[31] S. Yerolatsitis, F. Yu, S. McAughtrie, M. G. Tanner, H. Fleming, J. M. Stone, C. J. Campbell, T. A. Birks, and J. C. Knight, *Journal of Biophotonics*, **2019**, *12*, 3, e201800239.

[32] N. Krstajić, B. Mills, I. Murray, A. Marshall, D. Norberg, T. H. Craven, P. Emanuel, T. R. Choudhary, G. O. S. Williams, E. Scholefield, A.R. Akram, A. Davie, N. Hirani, A. Bruce, A. Moore, M. Bradley, and K. Dhaliwal, *Journal of Biomedical Optics*, **2018**, *23*, 7

[33] K. Ehrlich, A. Kufcsák, S. Mc.Aughtrie, H. Fleming, N. Krstajic, C. J. Campbell, R. K. Henderson, K. Dhaliwal, R. R. Thomson, and M. G. Tanner, *Opt. Exp.*, **2017**, *25*, 30976

[34] A. T. Erdogan, R. Walker, N. Finlayson, N. Krstajić, G. Williams, and J. Girkin, *IEEE Journal of Solid-State Circuits*, **2019**, *54*, 1705

[35] F. Yu, and J. C. Knight, *IEEE Journal of Selected Topics In Quantum Electronics*, **2016**, *22*, 1.

[36] M. H. Frosz, P. Roth, M. C. Günendi, and P. St.J. Russell, *Photonics Research*, **2017**, *5*, 88.

[37] T. Hassan, L. Thiberville, C. Hermant, S. Lachkar, N. Piton, F. Guisier, and M. Salaun, *PLoS ONE*, **2017**, *12*, 1.

[38] H. Wood, K. Ehrlich, S. Yerolatsitis, A. Kufcsák, J. Stone, T. Quinn, S. Fernandes, *University of Bath Research Data Archive,* **2022**, https://doi.org/10.15125/BATH-01174

[39] L. Thiberville, M. Saiaiin, S. Lachkar, S. Dominique, S. Moreno-Swirc, C. Vever-Bizet, and G. Bourg-Heckly, *European Respiratory Journal*, **2009**, *33*, 974.

[40] Norberg, Dominic, Source code and example data for "Open source image processing methods for real-time fibre bundle optical endomicroscopy", University of Edinburgh, College of Medicine and Veterinary Medicine, Deanery of Clinical Sciences, **2021**. https://doi.org/10.7488/ds/2960.

[41] S. Seth, A. R. Akram, P. McCool, J. Westerfeld, D. Wilson, S. McLaughlin, K. Dhaliwal, C. K. I Williams, *Scientific Reports*, **2016**, *6*, 31372.

[42] M. T. Gebrekidan, C. Knipfer, F. Stelzle, J. Popp, and S. Will, A. Braeuer, *Journal of Raman Spectroscopy*, **2015**, 47, 198.

[43] M. Wang, F. Tang, X. Pan, L. Yao, X. Wang, Y. Jing, J. Ma, G. Wang, and L. Mi, *BBA Clinical*, **2017**, *27*, 8.

[44] G. O. S. Williams, E. Williams, N, Finlayson, A. T. Erdogan, Q. Wang, S. Fernandes, A. R. Akram, K. Dhaliwal, R. K. Henderson, J. M. Girkin, and M. Bradley, *Nature Communications*, **2021**, *12*, 6616.

Graphical Abstract for Table of Contents

[Text: Design and experimental evaluation of a 1.4 mm diameter optical fibre endoscope probe enabling fluorescence endomicroscopy, time-resolved fluorescence spectroscopy, and Raman spectroscopy. The probe's bend limit, clinical practicality, and sensitivity to human lung tissue are investigated.

[Image: